Optical analysis of composite materials: metrological issues

Journal of Physics: Conference Series **3063** (2025) 012015 doi:10.1088/1742-6596/3063/1/012015

Optical analysis of composite materials: metrological issues

Luciano Chiominto[1*], Giulio D'Emilia[1], Emanuela Natale[1] and Francesco Tiberi[1]

[1] Department of Industrial and Information Engineering and Economics, University of L'Aquila, L'Aquila, Italy

[*]E-mail: luciano.chiominto@graduate.univaq.it

Abstract. In this paper, a procedure to improve the winding angle measurement of a filament winded composite component is proposed. The procedure is based on the use of a polarized camera that can acquire information on the direction of the light. This vision system has been proven to be suitable for the analysis of a carbon fibre surface due to the physical property of this material. It reflects light with a polarization angle equal to the orientation of the fibres. A statistical analysis of the angle of linear polarization (AoLP) for each pixel within the examined regions enables the evaluation of the winding angle. For improving this measurement, some geometrical and methodological aspects are examined in detail. A procedure for identifying a region of interest (RoI) in surface acquisition is proposed, and the impact of integrating multiple images of the same area is assessed. The result is a reduction in the variability of the measured distribution of the fiber angles.

1. Introduction

The adoption of carbon fiber-reinforced polymers (CFRPs) is expanding in various sectors such as automotive, aviation, marine, and civil engineering. This is thanks to the possibility of creating CFRPs components with high strength to weight ratio essential for various applications. Additionally, CFRPs offer a broad range of customizable material properties, allowing significant design flexibility in the final product [1]. Moreover, their mechanical performance, combined with high corrosion and fatigue resistance, makes them ideal for energy storage applications, including pressure vessels and generally for axial symmetric structures [2].

One of the most promising manufacturing processes for cylindrical structures like pipes or tanks is filament winding. This technique involves the systematic winding of resin-coated continuous filaments around a rotating mandrel in predetermined patterns to form an axial symmetric structure. When the desired thickness is reached, the composite structure undergoes a curing process, after which the mandrel is removed. The resulting in a hollow composite component [2-3]

In this process, the winding angle is a critical parameter that influences the mechanical characteristics of the final component. The angle between fibers is a critical parameter that must be controlled. For example, in [4] a 5° deviation in the orientation of non-crimp fabric composites (NCFC) could result in a 20% reduction in the component's strength. In addition to this, in the filament winding process minor variations of the pulling forces or anomalies in the deposition

head direction could lead to deviations in the mechanical characteristics or to defects inside the component structure. For example, voids, delaminations, and variations in thickness [5].

There are different Non-Destructive Techniques (NDT) used to characterize composite components and to study defects. The most used in literature are thermography, eddy current, ultrasonic, acoustic emission, shearography and Computed Tomography (CT) [6,7]. This is one of the most advanced inspection methods employed to study the structure of composite components. CT are used to evaluate and visualize the fibres of CFRP components. However, CT scanners have a great limitation in the size that could be inspected. This is a major drawback especially in the aerospace sector [8]. Even though it is not readily automated, another technique used to investigate fiber orientation in a composite component is Scanning Electron Microscopy (SEM) [9].

In general, All the above technologies enable the analysis of the finished part or after failure, but they are unable to offer direction or assistance during the manufacturing process. [10]

Compared to other inspection techniques, vision-based methods have several advantages such as the lack of interaction, small cost, and automation ease. Another important part of this system is the image processing algorithms [11,12].

Several vision-based inspection methods CFRPs weave exist. For example, direct optical methods use image analysis techniques like edge detection or gradient methods. Another advanced inspection system is bi-directional reflectance distribution function (BRDF) [13]. Here, the uppermost layer of the component is acquired synchronizing the sensor with the illumination system. Using different illumination patterns, it is possible to evaluate the fibers orientation by studying how light is reflected. As the author stated, for pre-pregs carbon fibers the root mean square error is in the order of 1.5°.

For the inspection of carbon fiber components using vision system, one of the most innovative techniques is the one based on polarization imaging. Polarization vision is a rapidly growing area within computer vision that focuses on capturing images with information about the polarization state of incoming light.

Different implementations of polarization vision exist in different fields. For example, it has been employed in photography for long time to reduce the effects of reflections and to improve visibility [14]. Other applications are in the High-Dynamic-Range (HDR) imaging [15], and to characterize bifringent fluids [16]. The application in the field of composite components inspection is still recent.

For composite components, It has been shown that carbon fibers reflect unpolarized light in a polarized manner with the same angle of the fiber orientation [17]. This physical property opened the possibility of characterizing CFRP weaves using polarization cameras.

In [17] a new polarization camera sensor is described. This is based on micro-filters on the sensor that acquire the light in four planes. Based on the pixel intensities it is possible to compute the Stokes parameters and the Angle of Linear Polarization (AoLP) with is oriented as the fibers. The polarization data processing let also to highlight different surface features [17,18] A polarization camera is utilized in [19] to examine various carbon fiber specimens, achieving sub-degree precision in the analysis of unidirectional materials, whether they are cured or dry-woven. The distribution of the fiber angle is also measured in [20] using a polarization camera on a Sheet Molding Compound material.

The winding angle measurement using polarization data was investigated in the previous work by the authors [10]. In that piece of research, the winding angle was evaluated considering

the fiber angle distribution of a single acquisition of a Region of Interest (RoI) that was manually defined.

To the best of authors knowledge, there is no research on approaches to improve the winding angle measurement reducing variability and noise. In this paper, an optimized method is proposed. The scope of this work is to study different methodologies to improve the winding angle measurement using a polarized vision system. The aspects explored are whether it is optimal to acquire repeated images of the same surface area. A method to identify a RoI for the study of non-planar components is also proposed.

2. Materials and Methods

2.1 Vision system

The surface of the component under analysis is captured using a FLIR Blackfly S BFS-PGE-51S5P camera. This is a monochrome camera polarization camera based on the Sony sensor IMX 250 CMOS. The camera native resolution is 2448 (H) × 2048 (W) pixels resulting in a total of 5.0 Mpixel.

The pixel dimensions are 3.45 μm, and each pixel is equipped with a four-direction polarizer integrated into the chip photodiode. This specialized design enables the simultaneous acquisition of polarization information across four distinct orientations. As shown in Fig. 1, the orientations of the polarization filters are 90°, 45°, 135° and 0°.

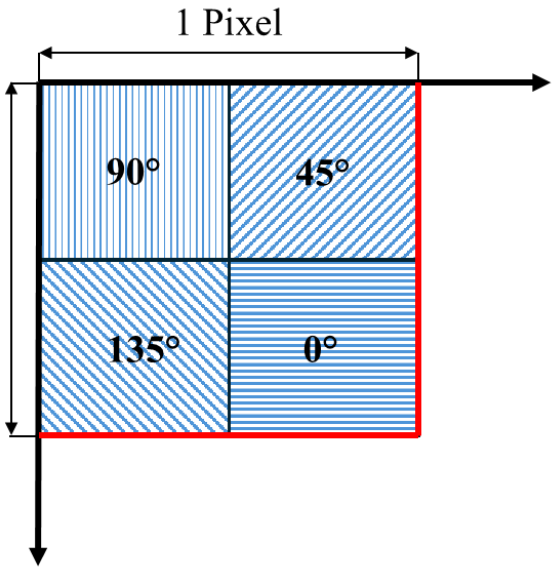

Figure 1. Polarization filters pattern on the Sony IMX250 CMOS sensor.

The illumination system employed is composed of two softboxes with 80W light bulbs. This system provides a uniform, diffused and unpolarized light source. Consequently, all the polarization information acquired by the camera is generated by the reflected light of the carbon fiber surface.

In this study, a 25 mm low-distortion lens is employed to achieve a balance between working distance and the minimization of perspective distortion.

A scheme of the vision system is represented in Fig. 2.

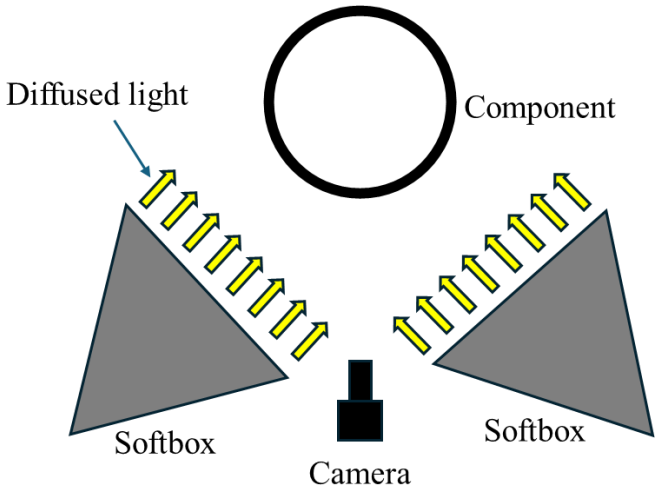

Figure 2. Scheme of the vision system.

As documented in another work by the authors [10], the results of the further analysis are influenced by the vision system settings. The studied factors are camera-piece distance, the distance between the light source and the component surface, lens aperture, and shutter speed. In the light of these results, the following settings are used for the acquisitions:

- 190 mm camera piece distance
- Softboxes positioned at 400 mm from the component surface
- f/8 of lens aperture
- 150 ms as shutter speed

The vision system is reported in Fig. 3.

Figure 3. Vision system used for the acquisitions.

2.2 Specimen under analysis

The investigation of non-planar components is the main goal of this work. For this reason, the specimen under analysis is a hollow cylinder that represents the central portion of a pressure vessel.

The materials used in the manufacturing process are commercially available. In particular, the carbon fiber used to produce the pre-preg tows is Toray T700S-12K-50C. For the resin system, Araldite LY 3508 as epoxy resin, Aradur 1571 as hardener, and Accelerator 1573 as accelerator are employed. All of these are produced by Huntsman Araldite.

The pre-preg tows are wound around a rotating mandrel by a deposition head. The final shape of the component is obtained by stacking different layers. The winding pattern used during the manufacturing process consists of an initial hoop layer in which the tows are wound at almost 90°. This preliminary step is necessary to encourage the adhesion of the ensuing helicoidal layers. The nominal winding angle of these is 60°.

As shown in Fig. 4, the resulting component is a hollow cylinder with an internal diameter of 200 mm and a length of 300 mm.

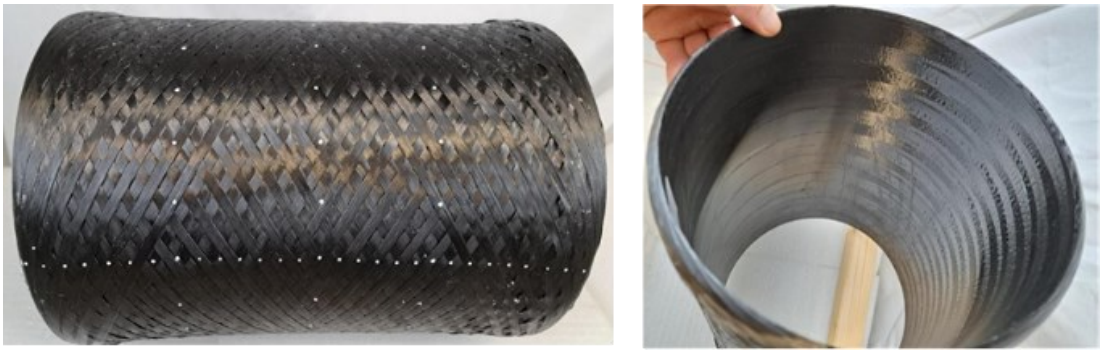

Figure 4. External and internal details of the filament winded hollow cylinder.

Fig. 5 represent the angles on a cylinder. The quantity of interest is the winding angle γ, which can be determined from the angle between the tows (2β). It is calculated performing the difference between 90° and the angle β.

2.3 Data processing

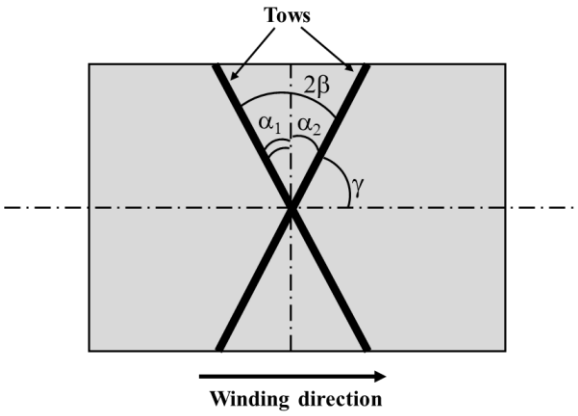

Figure 5. Winding angle from a helicoidal winding pattern.

Images are captured in RAW file format to retain all information from the camera sensor, utilizing Spinnaker SpinView acquisition software. Then, the acquisitions are imported into MATLAB for data processing.

The first step is the image "demosaic" process. The intensity values for each polarization orientation are extracted. As a result, there is an image for each polarization direction. The resulting images have a resolution equal to a quarter of the original one. In fact, the intensity images are 1224 (H) x 1024 (W) pixels.

Then, to describe the state of light polarization the Stokes parameters are computed. Considering the pixel intensity I for each direction θ, the Stokes parameters are determined considering the following formulas:

$$S_0 = \frac{I_0 + I_{45} + I_{90} + I_{135}}{2} \quad (1)$$

$$S_1 = I_0 - I_{90} \quad (2)$$

$$S_2 = I_{45} - I_{135} \quad (3)$$

Therefore, the Angle of Linear Polarization (AoLP) is computed using the following equation:

$$AoLP = 0.5 * \text{atan}\left(\frac{S_2}{S_1}\right) \quad (4)$$

Eq. 4 returns values in range [-90°; 90°] since it is calculated using the inverse tangent function. AoLP is also the parameter of interest since it aligns with fibre direction on the surface of the component under investigation. The output of this step is a matrix of the same dimensions of the intensity image and each element represents the AoLP value of each pixel.

Data are optimized to improve the winding angle measurement. The proposed methodology includes a RoI identification step and the combination of multiple images of the same area. Finally, the angle between tows, denoted as 2β in Fig.5, is computed by identifying the angles with maximum frequency, α1 and α2, and calculating the difference between these.All the data processing steps for an optimized winding angle measurement are summarized in Fig. 6

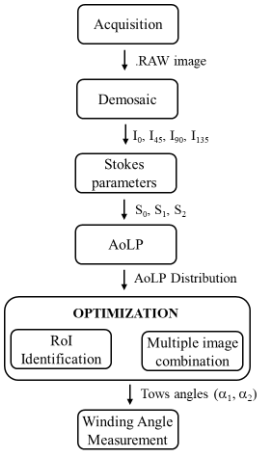

Figure 6. Scheme of the optimized data processing steps.

2.4 Measurement campaign

A portion of the cylinder surface is acquired twenty times without moving the object or changing the system settings. The acquisitions are combined computing the mean value of each pixel. Then, the following evaluations are made to improve the quality of the winding angle analysis:

- RoI identification
- Influence of combining acquisitions

2.5 RoI Identification

A correct RoI identification is a preliminary step before the evaluation of the winding angle. Since the component of interest is non-planar, the surface curvature could modify the light angle. In addition to this, the composite cylinder is cured, meaning that on the surface some resin residues are present and influence the angle of the reflected light.

Considering the AoLP matrix where each element is the mean value of the polarization angle of different acquisitions, the central column is used as a reference since the influence of the surface curvature is minimized. For the RoI identification the relative difference between the means of the standard deviations of each matrix column and the central one is computed.

2.6 Number of acquisitions

Adding one image at time, the acquisitions are combined by computing the mean value of each pixel. To study the influence of this procedure, the standard deviation of the fitted gaussian to the angle distribution is computed. The scope is finding a minimum number of acquisitions that reduces the standard deviation of the fitted gaussians without making the acquisition procedure too cumbersome and computationally heavy.

3. Results

3.1 RoI Identification

Fig. 7 reports the tows angles distribution and the fitted gaussians considering the whole acquisition.

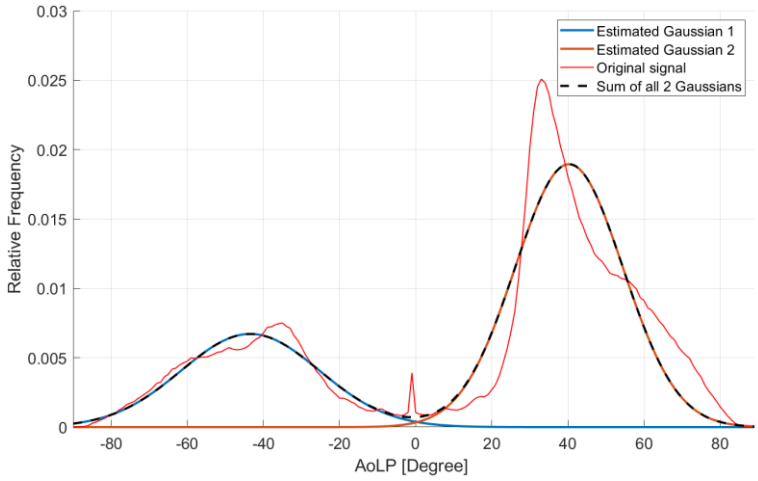

Figure 7. AoLP distribution of the whole acquisition.

As shown in Fig. 7, the tows angles are distributed along two main directions. Ideally, since the main tow's directions are two, these should be distributed as gaussians. However, considering the whole acquisition the AoLP values are not distributed accordingly. The fitted gaussian of the negative angle values is broad with a not defined angle of maximum frequency. Regarding the left distribution, this cannot be well represented as a gaussian for its shape. Considering the whole AoLP distribution, it seems as if the main angles directions are four and not two. The outermost distributions have greater mean values in absolute terms and lower frequency. This means that this behaviour is present on smaller zones of the acquisition that should be discarded and a RoI must be selected for the winding angle analysis.

Following the methodology described in the previous section, a RoI is identified. Fig. 8 represents the relative difference between the mean standard deviation of each column and the central one. The reference column is the one at the horizontal position of 612.

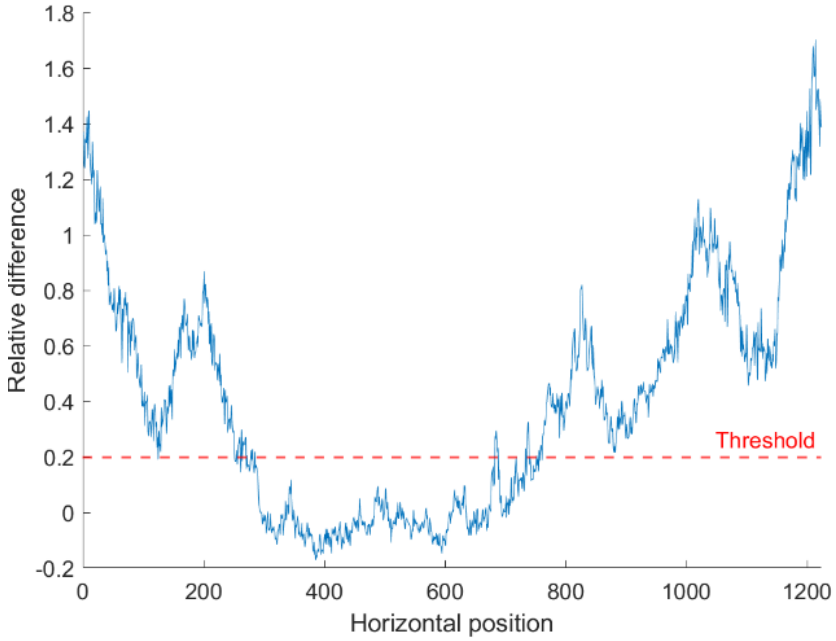

Figure 8. Relative difference between the AoLP of each column and the central one and the defined threshold for the RoI selection.

As shown in Fig. 8, the relative difference of each column depends on the horizontal position and ranges between -0.17 and 1.70. Moving from left to right, the relative difference starts from the maximum values and then decreases getting closer to the central part of the cylinder surface. In this area, relatively constant values are found. This is also the part where the relative difference is at the minimum. Then, it starts to increase again.

In this case, the region is identified defining a threshold equal to 0.2. All the columns with a relative deviation greater than the threshold are excluded from the analysis. As Fig.6 shows, the threshold identifies a RoI that starts from the horizontal position 286 to 751. In this case, the dimension of the RoI is about one third of the original image size.

The proposed method for finding a RoI is optimal for non-planar and cylindrical components. Considering each column of the AoLP matrix one-by-one permits to exactly identify in which

cylinder's generators the effect of the curvature starts to influence the AoLP measurement. With this approach, the corresponding RoI is represented in Fig. 9.

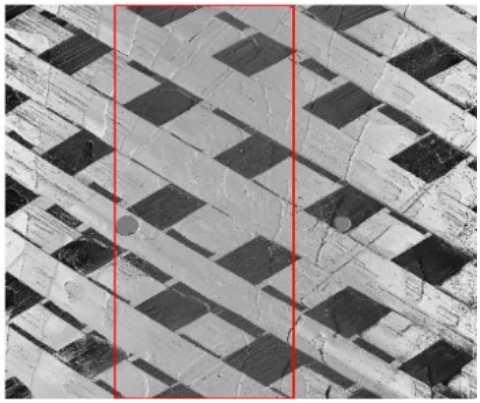

Figure 9. AoLP representation with the identified RoI.

After the RoI identification another two zones are defined. Zone 1 is on the left and Zone 2 is on the right of this region.

Extracting the AoLP values from the RoI is possible to evaluate the winding angle of the cylinder using the procedure described in the methodology section. Fig. 10 shows the distribution of the tows angle and the fitted gaussians.

As can be seen in Fig. 10, the tows angle orientations are correctly fitted using two gaussians. The maximum frequency angles are -37.0° and 32.6° correspondingly to the angles α_1 and α_2. The fitted distributions have respectively 9° and 6° as standard deviations. The distribution with higher variability is also the one with smaller amplitude since tows at -37.0° of orientation are less represented in the studied area of the cylinder.

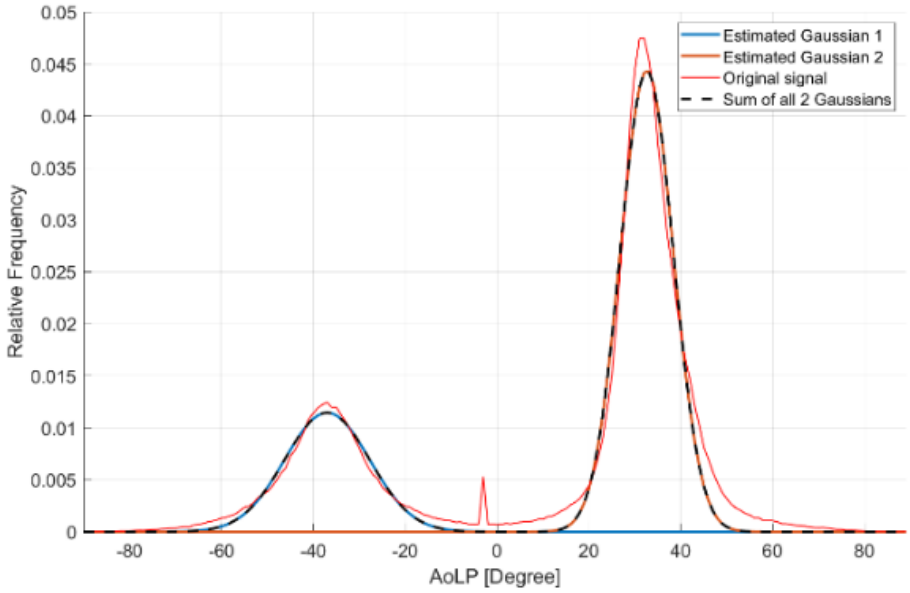

Figure 10. AoLP distribution and fitted gaussian of the identified RoI.

Tab.1 summarizes the angle of maximum frequencies for all zones of the image.

Table 1. Angles with maximum frequencies in the three defined zones of the acquisition.

	α_1 [°]	Dev 1 [°]	α_2 [°]	Dev 2 [°]
Zone 1	-57.4	19	54.7	14
RoI	-37.0	9	32.6	6
Zone 2	-49.6	16	47.8	17

As reported in Tab.1, the angles with maximum distribution in the RoI are smaller compared to the angles in the outer zones of the acquisition. This evidence validates that the surface of the cylinder influences the angle of polarization. In particular, the component curvature tends to modify the reflected polarized light angle increasing it. Moreover, the angles deviation in the RoI is less compared to the other zones, as highlighted in the previous analysis.

A RoI selection is a critical methodological aspect for a correct evaluation of the winding angle in non-planar components as filament wound cylinder.

3.2 Influence of the number of acquisitions

The distribution of the frequency of the AoLP values extracted from the RoI defined in the previous step is fitted using two gaussians. Performing the evaluation only on one image, the angle distribution and the determined gaussians are reported in Fig. 11.

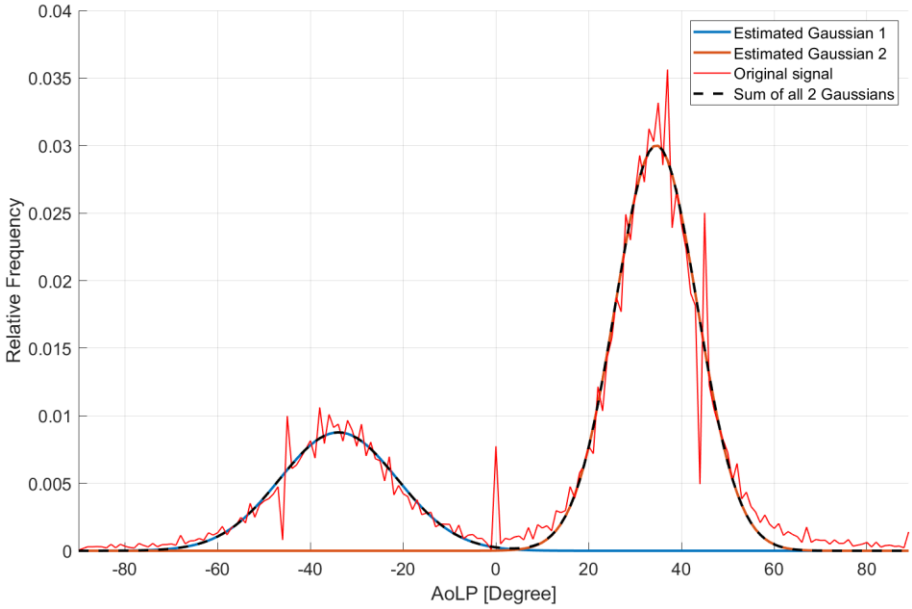

Figure 11. Fitting of the AoLP distribution on a single acquisition.

Fig.11 shows that the angles are distributed according to a bimodal distribution. The mode values of the two gaussians are -33.9° and 34.6° with 13° and 9° as standard deviations respectively.

In Fig.12 the trend of the standard deviations of the two fitted gaussians is reported. In each step an image is added to the previous ones. As specified in the previous section, for combining the images the mean of each AoLP element in the matrix is performed.

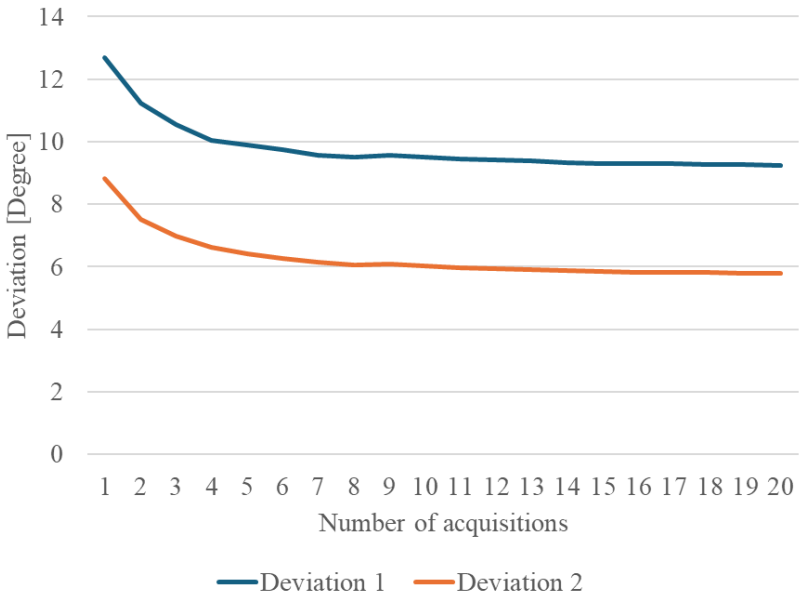

Figure 12. Deviations of the fitted gaussians combining more acquisitions.

As shown in Fig. 12, in the beginning there is a sharp decrease in the variability adding images. Adding images makes the variability of the fitted gaussians lower due to the reduction of noise. Even though the variability keeps decreasing, after six combined acquisitions the reduction is not so strong.

It must be pointed out that the quantity of interest is the angles with greater frequences since these determine the mechanical properties of the component. After the proposed optimization steps, the remaining variability of the angle distributions is due to the measurands themselves since tows are not perfectly planar and have a wrinkled surface. In addition to these characteristics, there are resin residues on the surface that influence the angle of the reflected light.

Considering the camera and the whole data processing, the initial reduction of resolution due to the combination of data from the different polarization directions seems to not impact the results. This is confirmed by the fact that even minor deformation of the tows are recognized.

4. Conclusions

In this paper the winding angle measurement of filament winded components is studied. A carbon fiber cylinder is analyzed using a vision system. This is based on a polarization camera that extracts the information of the direction of the reflected light to compute the tows angle. The winding angle is calculated fitting the distribution of the tows angle in a RoI with two gaussians.

Some geometrical and methodological aspects are explored in-depth. A procedure to identify a reduced RoI in the surface acquisition is proposed and the influence of combining more images of the same area is evaluated.

To further reduce variability, combining more acquisitions and performing the mean provides a reduction of the variability of the fitted gaussians. A threshold of the requested images is also identified.

In conclusion, assessing the winding angle of composite components using a polarization camera is a promising approach for process control, allowing precise angle measurements. However, there is always a residual variability of the angle distribution due to the tows characteristics and the presence of resin residues on the surface.

Further work will be devoted to improve the analysis of variability causes.

References

[1] Das T K, Ghosh P and Das N Ch 2019 Preparation, development, outcomes, and application versatility of carbon fiber-based polymer composites: a review Adv Compos Hybrid Mater 2 214–33
[2] Azeem M, Ya H H, Alam M A, Kumar M, Stabla P, Smolnicki M, Gemi L, Khan R, Ahmed T, Ma Q, Sadique M R, Mokhtar A A and Mustapha M 2022 Application of Filament Winding Technology in Composite Pressure Vessels and Challenges: A Review Journal of Energy Storage 49 103468
[3] Antunes M B, Almeida Jr J H S and Amico S C 2020 Curing and seawater aging effects on mechanical and physical properties of glass/epoxy filament wound cylinders Composites Communications 22 100517
[4] Vallons K, Duque I, Lomov S and Verpoest I Fibre orientation effects on the tensile properties of biaxial carbon/epoxy NCF composites vol ICCM International Conferences on Composite Materials
[5] Natale E, Gaspari A, Chiominto L, D'Emilia G and Stamopoulos A G 2024 Morphological analysis of as-manufactured filament wound composite cylinders using contact and non-contact inspection methods Engineering Failure Analysis 158 108011
[6] Gupta R, Mitchell D, Blanche J, Harper S, Tang W, Pancholi K, Baines L, Bucknall D G and Flynn D 2021 A Review of Sensing Technologies for Non-Destructive Evaluation of Structural Composite Materials Journal of Composites Science 5 319
[7] Wang B, Zhong S, Lee T-L, Fancey K S and Mi J 2020 Non-destructive testing and evaluation of composite materials/structures: A state-of-the-art review Advances in Mechanical Engineering 12 1687814020913761
[8] Nelson L J, Smith R A and Mienczakowski M 2018 Ply-orientation measurements in composites using structure-tensor analysis of volumetric ultrasonic data Composites Part A: Applied Science and Manufacturing 104 108–19
[9] Zheng T, Guo L, Sun R, Li Z and Yu H 2021 Investigation on the compressive damage mechanisms of 3D woven composites considering stochastic fiber initial misalignment Composites Part A: Applied Science and Manufacturing 143 106295
[10] Chiominto L, D'Emilia G and Natale E 2024 Using Light Polarization to Identify Fiber Orientation in Carbon Fiber Components: Metrological Analysis Sensors 24 5685
[11] Şerban A 2016 Automatic detection of fiber orientation on CF/PPS composite materials with 5-harness satin weave Fibers Polym 17 1925–33
[12] D'Emilia G, Gaspari A, Natale E, Stamopoulos A G and Di Ilio A 2022 Experimental and numerical analysis of the defects induced by the thermoforming process on woven textile thermoplastic composites Engineering Failure Analysis 135 106093
[13] Zambal S, Palfinger W, Stöger M and Eitzinger C 2015 Accurate fibre orientation measurement for carbon fibre surfaces Pattern Recognition 48 3324–32
[14] Namer E and Schechner Y Y 2005 Advanced visibility improvement based on polarization filtered images Polarization Science and Remote Sensing II Polarization Science and Remote Sensing II vol 5888 (SPIE) pp 36–45
[15] Wu X, Zhang H, Hu X, Shakeri M, Fan C and Ting J 2020 HDR Reconstruction Based on the Polarization Camera IEEE Robotics and Automation Letters 5 5113–9
[16] Lane C, Rode D and Rösgen T 2021 Optical characterization method for birefringent fluids using a polarization camera Optics and Lasers in Engineering 146 106724
[17] Schöberl M, Kasnakli K and Nowak A Measuring Strand Orientation in Carbon Fiber Reinforced Plastics (CFRP) with Polarization

[18] D'Emilia G, Chiominto L, Natale E and Stamopoulos A 2024 Improving the Winding Angle Measurement for an Effective Process Control 2024 IEEE International Instrumentation and Measurement Technology Conference (I2MTC) 2024 IEEE International Instrumentation and Measurement Technology Conference (I2MTC) pp 1–6
[19] Atkinson G A, O'Hara Nash S and Smith L N 2021 Precision Fibre Angle Inspection for Carbon Fibre Composite Structures Using Polarisation Vision Electronics 10 2765
[20] Schommer D, Duhovic M, Hoffmann T, Ernst J, Schladitz K, Moghiseh A, Gortner F, Hausmann J, Mitschang P and Steiner K 2023 Polarization imaging for surface fiber orientation measurements of carbon fiber sheet molding compounds Composites Communications 37 101456